# Mechanical Analysis of Road Graben Slopes Based on Saturated-Unsaturated Seepage Theory

Li Peijun, Lu Hao* and Li Qing

*Guangdong Transportation Technology Testing Co., Ltd., Guang Zhou Guangdong 510550, China*
*E-mail: lhchd0220@126.com*
**Corresponding Author*

Received 21 August 2023; Accepted 06 September 2023;
Publication 30 September 2023

## Abstract

As the construction of mountainous highways continues to heat up, the stability analysis of road graben slopes becomes one of the current research hotspots. In this paper, based on the saturated-unsaturated seepage theory, the force analysis of the road graben slope under rainfall conditions and its laws are studied. Firstly, the damage mode of the road graben slope and its three damage stages of creeping deformation, sliding damage and tendency to stability are summarized according to the engineering practice and literature survey, and the right side of the road graben slope from K316+439 to K316+859 of Longlian Expressway is monitored, so as to amend the next theoretical analysis. The three stages of rainfall infiltration were analyzed, the state variables and material variables of soil water were selected according to the continuous medium theory and the soil water suction analysis was carried out. Based on the saturated-unsaturated seepage theory, the fluid-structure interaction mathematical model and soil moisture characteristic curve (SWCC) model under rainfall infiltration conditions were established, and the stress of the cutting slope under saturation conditions was analyzed.

*European Journal of Computational Mechanics, Vol. 32_3,* 285–312.
doi: 10.13052/ejcm2642-2085.3234

The experimental results show that for the soil at the foot of the slope, the infiltration depth of rainfall is limited due to the low permeability coefficient, and the change of seepage field is not obvious; the longer the rainfall is held, the deeper the infiltration depth is, and the rainfall will continuously replenish the groundwater, so the force on the slope of the road graben will increase continuously and finally reach the limit of damage. When the rainfall intensity is 5mm-h-1, the decline of stability coefficient for 48 h is 0.121; the initial stability coefficient of the slope is the largest when the dip angle of the weak interlayer is equal to 25°, and the stability coefficient decreases rapidly with the rainfall time, and when the rainfall reaches 60 h, the stability coefficient tends to be stable and the equilibrium of the slope force no longer changes.

**Keywords:** Force analysis, soil water suction, creeping deformation, saturated-unsaturated seepage theory, stability.

## 1 Introduction

In mountainous and hilly areas, because of atmospheric rainfall, sudden earthquakes and other factors, it is often easy to appear slope instability, but rainfall is relatively the most common type of influencing factors. Especially in the southern region of China, the long rainy season and frequent rainstorms have a greater impact on slope stability [1]. Therefore, natural disasters such as landslides and mudslides are also closely related to rainfall and rainwater, and a lot of work has been done on rainfall infiltration and slope stability, but the law and influence of rainfall infiltration in unsaturated zones need to be further summarized. Under the action of rainfall infiltration, the seepage field in the soil mainly changes. During rainfall, the soil will approach from unsaturated to saturated, so that the shear strength of unsaturated soil decreases due to the increase of water content in the soil [2]. At the same time, the pore water pressure in the soil increases, and the substrate suction decreases, which greatly reduces the stability of the slope, and eventually leads to the instability of the slope.

At present, based on rock-saturated-unsaturated seepage theory, Yang Xin used Go-studio finite element software to establish a numerical calculation model for high slopes containing soft and weak inclusions, and carried out a study on seepage characteristics at the top, middle and bottom locations of high slopes containing soft and weak inclusions in road graben under different rainfall factors [3]; Pan H proposed the utility of the Pan H proposed

the software of the coupled dynamic mannequin of multi-body gadget in the comparison of action posture stability, mounted the coupled dynamic mannequin of human action posture and accumulated the applicable records of human action posture [4]; Xu Haitao et al. used saturation-unsaturation theory to establish a coupled flow-solid model under rainfall infiltration conditions, obtained the distribution of the transient saturation zone and stress field of the cascade slope under different rainfall calendar conditions, and analyzed the damage mechanism of the cascade slope under continuous rainfall conditions, and obtained the corresponding safety factor of the slope [5]; Paul K et al. proposed a strong cylindrical gap in a uniform magnetic subject appearing in the route of the axis of the cylindrical gap and the time scheme of the laser beam was once viewed non-Gaussian and acted on the floor of the cylindrical gap [6]; Yu Jinhui picked up the numerical simulation of the seepage characteristics of the high road graben slope under the effect of heavy rainfall by using the finite element calculation software, and obtained the change law of its internal seepage field, based on the principle of effective stress of unsaturated soil and the simplified Bishop method to obtain the change trend of the safety coefficient of the high road slope under the condition of heavy rainfall [7]; The new algorithm proposed via Rezaiee-Pajand M et al. is in a position to pass by the load and displacement restriction factors of quite a number benchmark troubles with extreme nonlinear conduct and the proposed technique has the quickest convergence price in contrast to the regular plane, up to date everyday aircraft and cylindrical arc size techniques [8].

As the construction of mountainous highways continues to heat up, the stability analysis of road graben slopes becomes one of the current research hotspots. In this paper, according to the saturated-unsaturated seepage theory, the force analysis of the road graben slope under rainfall conditions and its laws are studied. Firstly, the damage mode of the road graben slope and its three damage stages of creeping deformation, sliding damage and tendency to stability are summarized according to the engineering practice and literature survey, and the right side of the road graben slope from K316+439 to K316+859 of Longlian Expressway is monitored, so as to amend the next theoretical analysis. The three stages of rainfall infiltration were analyzed, and the state variables and material variables of soil water were selected according to the continuous medium theory and the soil water suction analysis was carried out, and the flow-solid coupling mathematical model and soil water characteristic curve (SWCC) model under the rainfall infiltration conditions were established according to the saturated-unsaturated seepage theory with

the continuity assumption. The experimental results show that for the soil at the foot of the slope, the infiltration depth of rainfall is limited due to the low permeability coefficient, and the change of seepage field is not obvious; the longer the rainfall is held, the deeper the infiltration depth will be, and the rainfall will continuously replenish the groundwater.

## 2 Slope Damage Model and Monitoring of Road Graben

### 2.1 Destruction Patterns and their Stages

Engineering practice shows that when sliding damage of roadside slopes occurs, the damage surface is often partly tracing the structural surface and partly cutting through the soil, and its damage sliding surface is usually a combination of circular arc and straight line [9]. The literature investigated 45 cases of granite residual soil destabilization slopes, and the statistical results are shown in Table 1. It can be seen that the primary and secondary structural surfaces play a decisive role in the slope destabilization of granite residual soil [10]. Among them, Type II damage form is in the form of iterative tile, and its prograde and damage surface are nearly vertical. The slopes of the road graben all have larger slope rates, and their destabilization damage forms are basically all Type I.

According to the literature and the location and yield of the primary structural surface, the damage of Class I graben slopes can be summarized into four basic types, as shown in Figure 1: upper rounded and lower straight (A), upper straight and lower rounded (B), both ends rounded and middle straight (C), upper and lower straight and middle rounded (D).

Morphologically, the damage types of slopes are mainly divided into two kinds of collapse and landslide: Collapse damage mainly occurs in rocky slopes, where the blocky rock body separates from the slope body and rolls down along the slope surface. During the process of collapse, the rock body does not have an obvious slip surface. This type of damage is likely to occur in the leading edge zone of high and steep slopes [11]. A landslide is an overall sliding of a rock and soil body along a weak surface within a slope

**Table 1** Types of destabilized slope damage

| Type of Damage | I | II | III | IV |
|---|---|---|---|---|
| Form of damage | Sliding along the native structural surface | Sliding along secondary structural surfaces | Collapse | Sliding along a circular surface |
| Proportion | 43 | 36 | 16 | 5 |

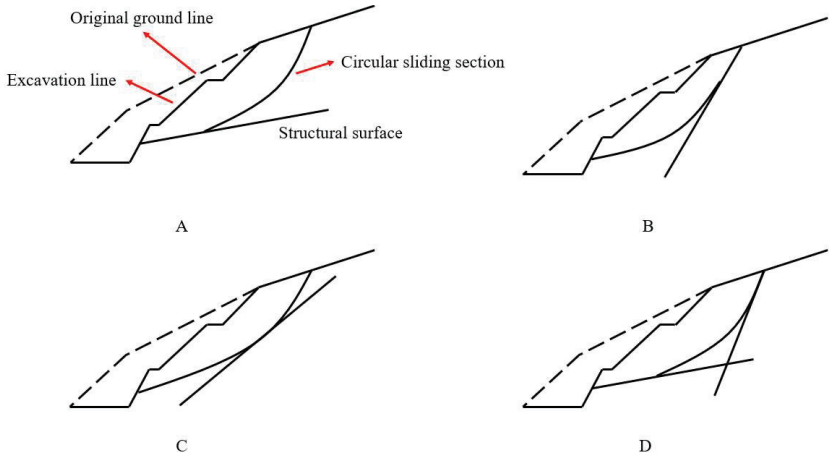


**Figure 1** Slope damage pattern of road graben.

under the action of gravity [12]. The actual form of damage of slopes is quite complex, and there are many forms of damage between the above two forms, such as landslide, spalling, flow, etc. There may also be a combination of several forms of damage.

The damage process of slopes can be classified into three phases:

The first stage is the creeping transformation stage of the rock body of the slope, in this state cracks will generally appear on the slope surface and the top of the slope, and the cracks will increase in size gradually.

The second stage is the sliding destruction stage of the slope, the back edge of the sliding rock body sinks rapidly, and the sliding rock and soil body slides down at a fairly fast speed, this stage is the most dangerous stage, which may cause great harm.

The third stage is the stage of stability, after the sliding stage, the loose rock and soil body is gradually compacted, and the slope is slowly destabilized.

## 2.2 Slope Monitoring Content of Road Graben

Longlian Expressway starting point K206+222 in Longchuan County Lao Long town and has been opened to the Meihe Expressway, the end point K334+200 is located in Shaoguan City, Longyuan County, Long Xian Town, Tangxia Village, the total length of the route 127.978 km. K316+439 $\sim$ K316+859 right ten rift valley slope is a large landslide deformation slope,

the slope geological condition and environment is more complex, rich in groundwater. The slope was originally set up as a four-stage slope, and in December 2016, destabilization and decline occurred during the construction of slope support, and then the design was changed to adopt the landslide treatment plan of large-scale load reduction + strong support, and the slope still experienced shear displacement after the construction of the changed design.

According to the historical monitoring of this slope and some problems existing after the change of treatment, the main purpose of this monitoring is as follows:

1. To investigate the safety hazards, promote the slope "prevention-oriented, treatment early treatment small" preventive maintenance virtuous cycle, improve the economic efficiency of highway operation.
2. Improve the quality of road slope maintenance and service level, improve the efficiency of maintenance personnel, realize the principle of maximizing the benefits of maintenance funds, and ensure the safe operation of road slope without interrupting the traffic.
3. Discover the major disease signs of this slope in time, analyze and predict the possibility of sudden disasters, report them in time, and provide preliminary remediation suggestions [13].
4. Through the long-term monitoring of the slope, the deformation and development of the slope are mastered, and then the reinforcement treatment effect is analyzed, so as to accumulate the treatment experience for the subsequent project, and provide a basis for the standardization and scientific management of highway slope maintenance.

In order to achieve the purpose of slope monitoring, the real deformation trend of the slope is accurately reflected within the monitoring period as far as possible. According to the requirements, it is proposed to monitor the deep horizontal displacement of the slope along the existing inclined holes, and the specific monitoring points are laid out as Figure 2. The main work content of this monitoring period includes: slope disease investigation and deep horizontal displacement monitoring.

### 2.3 Rainfall Conduction Process

During the rainfall ingress process, rainfall penetration follows a specific trajectory of movement. In the case of specific geotechnical slopes, the unsaturated soil has a limited depth, where the saturated soil is located in the area below the unsaturated soil [14]. The process of rainfall infiltration

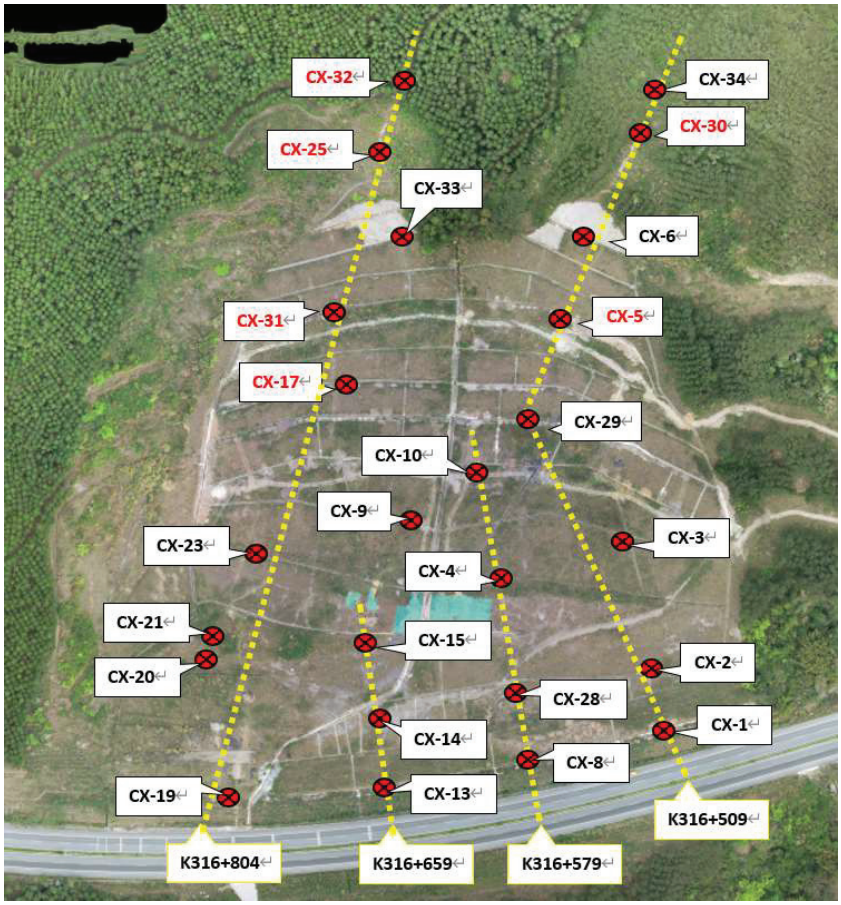


**Figure 2** Layout of deep horizontal displacement monitoring points of road graben slope.

from the appearance of the soil body to the interior of the soil body during rainfall is very complex. Rainfall from the slope surface soil body slowly infiltration, gradually fill the void inside the soil body, and the soil body in the gas discharge, when all the gas in the void of the soil body is discharged, the soil body tends to be saturated, and at this time the water content that is the saturated water content. If the rainfall per unit of time is greater than the infiltration rate, a certain amount of rainfall will enter the soil along the cracks of the soil body, and the residual rainfall will be pooled into runoff on the slope surface and accumulated at the foot of the slope; however, if the rainfall continues to penetrate into the soil, the amount of infiltration

will slowly decrease to reach the constant volume of infiltration [15]. If the amount of rainfall per unit time is greater than the infiltration amount, the rainfall will enter into the soil. Because of the continuous entry of rainfall, the soil gradually becomes saturated, however, the saturated infiltration of rainfall into the soil will be affected by the initial water content. Therefore, the process of rainfall infiltration is gradual and shows a certain change pattern in the process of infiltration.

Many scholars have conducted a lot of experimental studies on the infiltration process of rainfall on the slope. During the course of rains, the trend of rainfall penetration to the soil on the slope is a decreasing curve, which can be divided into 3 processes. First, in the earlier phase of rains, due to the small water content in the soil, there are many voids in the soil. Therefore, rainwater can enter into the soil in large quantities, and the infiltration effect at this moment shows a relatively fast trend [16]. After a period of rainfall, along with the continuous reduction of voids in the soil, the rate of rainwater infiltration is gradually reduced, and the effect of rainwater infiltration will gradually decrease, as long as it is not yet in a saturated state, rainfall will still appear to flow into the soil. If the rainfall exceeds a certain amount, then the rainwater will completely fill all the voids in the soil, rainwater infiltration rate also tends to stabilize, if in a saturated state, the soil is in a saturated state, and the soil water content is at its maximum value at this moment, and the value is the sitting water content.

By combining the existing theoretical calculations and related studies, the calculation of the infiltration rate of rainwater, the amount of water entering into the unit area per unit of time can be calculated, which is equivalent to the total infiltration in that soil body. Expressions are as follows:

$$i(t) = q(0,t) = -k(h)\frac{\partial(h+z)}{\partial z} = -\,k(h)\left(\frac{\partial h}{\partial z}+1\right)\Bigg|_{z=0} \tag{1}$$

Among them: *h* is different in value, and the matrix potential and pressure head are respectively in unsaturated soil and saturated soil.

Coleman and Bodman obtained through their study that rainwater gradually infiltrates from the surface of dense entities, and usually the water content can be divided into four regions from the surface to the inside, saturated zone, transition zone, conduction zone and wetting zone. And the wetting front refers to the leading edge of the wetting zone, as in Figure 3.

Each zone has the following characteristics:

a. Saturation zone: by the filling of water, the pores in the soil tend to be saturated, and the water content in this area is mainly affected

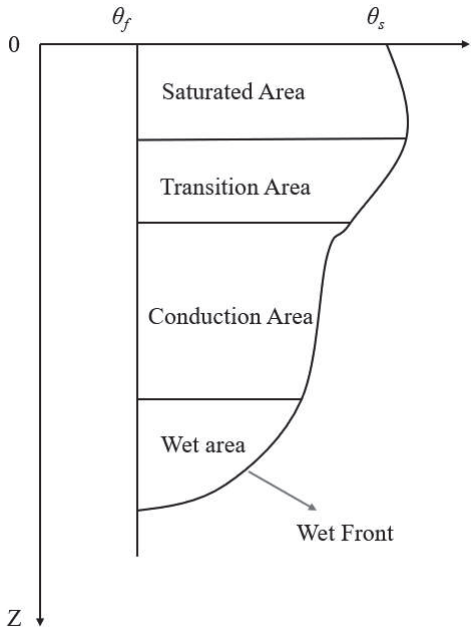


**Figure 3** Soil rainwater infiltration zoning.

by infiltration parameters, rainfall time, rainfall intensity and other factors [17].

b. Transition zone: With the increase of soil depth, the moisture content gradually decreases, which needs to be calculated in combination with simulation tests, and can also be simulated by V-G model.
c. Conduction zone: The moisture content is almost not affected by the change of soil depth, and it is an unsaturated zone with large water content and deep depth in the soil.
d. Wet zone: With the increase of soil depth, the moisture content gradually decreases and gradually approaches the initial water content.
e. Wet front: belongs to the dividing line between dry soil and wet soil, with different hydraulic gradient values.

## 3 Stability Analysis of Rainfall Infiltration Slopes

### 3.1 Continuity Assumptions

Soil is a complex discrete medium with three phases, and the soil, water and air that make up its three phases all participate in the natural cycle, and in the

process of circulation, groundwater stored in soil, rock pores, rock fractures or pores will be transported according to different pore conditions [18]. As water migrates, the size, shape, and connectivity of pores in the soil change. Thus, the three phases in the soil are in a state of mutual influence and coupling all the time. How to effectively simulate the structure of a porous medium like soil and the flow of fluid in its pore yard is the key to analyzing the saturated non-saturated seepage and stability of soil. This problem can usually be studied through both microscopic and macroscopic approaches, by formulating hypotheses and building models:

(1) Microscopic aspects: some scholars consider the soil as a collection of small spheres or hypothetically as a collection of small parallel flat bodies, but more commonly, soil pores are approximated as capillaries of varying diameters [19]. Although these microscopic models provide a more reasonable explanation of soil seepage in terms of principle, they inevitably oversimplify and approximate the soil, and therefore have little practical value [20].

(2) Macroscopic aspects: It is the study of the pore size of porous media and the average condition of its water flow in a larger scale. Generally in the soil body can take a volume element with *P* point as the center of mass and volume $\Delta V_i$, located in this volume element, the total volume occupied by the pores is $\Delta V_{vi}$, then the ratio can be determined:

$$n_i = \Delta V_{vi} / \Delta V_i \tag{2}$$

According to the research of the scholars, $n_i$ has the relationship with $\Delta V_i$ as shown in Figure 4:

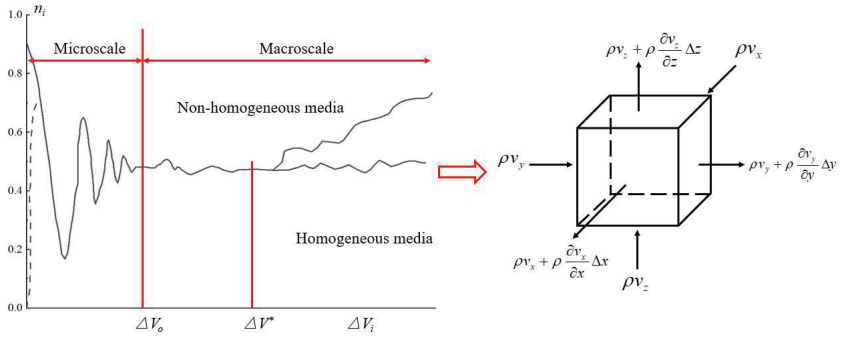


**Figure 4** $n_i$ versus $\Delta V_i$ curve.

From Figure 4, it can be seen that $n_i$ varies with $\Delta V_i$, and there exists such a critical point for its value. When $\Delta V_i$ decreases to a certain value, there is a clear cut-off in the value of $n_i$ at this critical point, and the value of $n_i$ varies around this critical point. Therefore, it can be assumed that there exists such a limit, i.e.:

$$n(p) = \lim_{\Delta V_i \to \Delta V_0} \frac{\Delta V_{vi}(P)}{\Delta V_i} \tag{3}$$

Call the volume element with volume $\Delta V_o$ at this point as the physical point of the porous medium at point $P$. $n(P)$ is the porosity at point $P$. Similarly, all other physical parameters of the earth can be specified as a continuous function of the location $P$. In this way, the actual porous medium is treated as a hypothetical continuous medium.

Following the assumptions obtained from the above macroscopic approach, the pore flow of water in the real earth can be considered as the continuous flow of water that fills the entire space and the individual elements of the flow can also be defined at the physical point $P$ [21]. For example, the flow velocity $v$ in the axial direction can be defined as

$$v = \lim_{\Delta V_i \to \Delta V_0} \frac{1}{\Delta A_i} \int_{\Delta A_i} u dA_v \tag{4}$$

Where, $\Delta A_{vi}$ is the area occupied by the gap on the cross-sectional area $\Delta A_i$ in the porous medium. If the average flow rate of the real water flow in the porosity space is expressed, the relationship between the permeate flow speed $v$ and the average flow speed of the pore space can be derived according to the definition of this volume element above as

$$v = nu_{cp} \tag{5}$$

When the pore water flow in a porous medium is replaced by a hypothetical continuous water flow, the kinematic elements such as flow velocity and flux and the kinematic parameters such as hydraulic conductivity can be regarded as continuous functions of the position *P*(*x*,*y*,*z*). Through the above analysis, a continuous soil medium model equivalent to the discrete soil body is then established, and a continuous functional form of the physical parameters of the earth body and the relevant control variables of seepage is proposed.

### 3.2 Seepage Equations for Saturated-Unsaturated Soils

According to the above continuity assumption, the seepage equation of unsaturated soil will be derived below.

Consider the flow of water in a micro-element whose lengths in three directions are assumed to be $\Delta x$, $\Delta y$ and $\Delta z$, respectively, as shown in Figure 4.

$$\rho v_y + \rho \frac{\partial v_y}{\partial y} \Delta y$$

Take the unit abcdefgh, the volume of the unit is $\Delta x \Delta y \Delta z$, assume that the flow velocity of each point on the six faces of the soil unit is equal, the flow velocity in each direction are $v_x$, $v_y$, $v_z$, then the mass of water flowing into the unit at $t \sim t + \Delta t$ is:

$$m_{in} = \rho v_x \Delta y \Delta z \Delta t + \rho v_y \Delta x \Delta z \Delta t + \rho v_z \Delta x \Delta y \Delta t \tag{6}$$

The mass of water flowing out is:

$$\begin{aligned} m_{out} = {} & \rho \left( v_x + \frac{\partial v_x}{\partial x} \Delta x \right) \Delta y \Delta z \Delta t + \rho \left( v_y + \frac{\partial v_y}{\partial y} \Delta y \right) \Delta x \Delta z \Delta t \\ & + \rho \left( v_z + \frac{\partial v_z}{\partial z} \Delta z \right) \Delta x \Delta y \Delta t \end{aligned} \tag{7}$$

The difference in the quality of the water draining into the outflow earth cell is:

$$\Delta m = m_{in} - m_{out} = -\rho \left( \frac{\partial v_x}{\partial x} + \frac{\partial v_y}{\partial y} + \frac{\partial v_z}{\partial z} \right) \Delta x \Delta y \Delta t \tag{8}$$

Assuming that the volume water contained in the soil is $\theta$, the variation of the mass of the soil unit body in time $\Delta$ is obtained from Equation (8) as:

$$\Delta m = \rho \frac{\partial \theta}{\partial t} \Delta x \Delta y \Delta t \tag{9}$$

Assuming that the water cannot be compressed deformation, known by the law of conservation of mass, Equations (8), (9) is equal, thus obtaining the following formula:

$$\frac{\partial \theta}{\partial t} = - \left( \frac{\partial v_x}{\partial x} + \frac{\partial v_y}{\partial y} + \frac{\partial v_z}{\partial z} \right) \tag{10}$$

If a condition (boundary flow $Q$) is imposed on the soil cell boundary, Equation (10) becomes:

$$\frac{\partial \theta}{\partial t} = -\left(\frac{\partial v_x}{\partial x} + \frac{\partial v_y}{\partial y} + \frac{\partial v_z}{\partial z}\right) + Q \tag{11}$$

The seepage velocity in each direction of three-dimensional seepage in unsaturated soils can be obtained according to equation:

$$v_x = -k_x(\theta)\frac{\partial h}{\partial x}, v_y = -k_y(\theta)\frac{\partial h}{\partial y}, v_z = -k_z(\theta)\frac{\partial h}{\partial z} \tag{12}$$

Substituting this into Equation (11) yields:

$$\frac{\partial \theta}{\partial t} = \frac{\partial}{\partial x}\left(k_x(\theta)\frac{\partial h}{\partial x}\right) + \frac{\partial}{\partial y}\left(k_y(\theta)\frac{\partial h}{\partial y}\right) + \frac{\partial}{\partial z}\left(k_z(\theta)\frac{\partial h}{\partial z}\right) + Q \tag{13}$$

Usually, when analyzing seepage in unsaturated soils, we tend to consider two-dimensional seepage, considering water infiltration in both horizontal and vertical directions, then the above equation can be rewritten as:

$$\frac{\partial \theta}{\partial t} = \frac{\partial}{\partial x}\left(k_x(\theta)\frac{\partial h}{\partial x}\right) + \frac{\partial}{\partial z}\left(k_z(\theta)\frac{\partial h}{\partial z}\right) + Q \tag{14}$$

The permeability coefficient of non-saturated soil is a variable related to the volume water contained $\theta$. Therefore, Equation (14) is actually a nonlinear partial differential equation, and it is usually hard to get the analytical answer of this nonlinear differential equation, so in practice we often solve this equation by numerical methods.

In 1978 Fredlund and Morgenstern proposed to use net stress $(\sigma - u_a)$ and matrix suction $(u_a - u_w)$ to describe the stress state of unsaturated soils. It was also considered that the variation of the volume water contained in unsaturated soil is the result of the joint action of the net force and the matrix absorption, and the expressions are

$$d\theta = -m_1^w d(\sigma - u_a) - m_2^w d(u_a - u_w) \tag{15}$$

It is assumed that no loading and unloading of the soil occurs during the saturated-unsaturated soil transient seepage calculations at each specific time step. That is, $\sigma$ is a fixed value and it is assumed that the gas in the unsaturated region of the soil is always continuous, i.e., the porosity stress

is always kept at a fixed atmospheric pressure [22]. Therefore, $(s - u_a)$ also remains constant, so the change in net stress has no effect on the change in bulk water content. Based on the above assumptions, the differential equation for seepage in unsaturated soils is

$$d\theta = -m_2^w d(u_a - u_w) \tag{16}$$

Bringing Equation (16) into (14) yields:

$$-m_2^w \frac{\partial(u_a - u_w)}{\partial t} = \frac{\partial}{\partial x}\left(k_x(\theta)\frac{\partial h}{\partial x}\right) + \frac{\partial}{\partial z}\left(k_z(\theta)\frac{\partial h}{\partial z}\right) + Q \tag{17}$$

From Equation (16), it is known that at this time $m_2^w = -\frac{\partial\theta}{\partial(u_a - u_w)}$, which is the slope of the soil-water characteristic curve.

Total water head $h = z + \frac{u_w}{\gamma_w}$, $u_w = \gamma_w(h - z)$, also due to $\frac{\partial z}{\partial t} = 0$, $\frac{\partial u_a}{\partial t} = 0$, $\partial\theta = -m_2^w \partial(u_a - u_w)$.

So $\frac{\partial\theta}{\partial t} = m_2^w \frac{\partial u_w}{\partial t} = \gamma_w m_2^w \frac{\partial h}{\partial t}$, substitute into Equation (14)

$$\gamma_w m_2^w \frac{\partial h}{\partial t} = \frac{\partial}{\partial x}\left(k_x(\theta)\frac{\partial h}{\partial x}\right) + \frac{\partial}{\partial z}\left(k_z(\theta)\frac{\partial h}{\partial z}\right) + Q \tag{18}$$

The equation is a two-dimensional transient seepage control equation.

### 3.3 Status Variables

When describing phenomena occurring in nature or in engineering practice, we often have to study them by means of establishing state variables, so state variables can be considered as a kind of covariate that requires an all-round description of the systematic state of the phenomenon at hand [23]. The state variables commonly used in saturated-unsaturated seepage theory include hydraulic head, effective stress, etc.; while soil material variables include modulus of elasticity, permeability coefficient, etc., which are an inherent property of the material and depend on the type of material.

According to the macroscopic or apparent form in the framework of the theory of mechanics and thermodynamics of continuous media, the state variables are not independent from the material variables, but scholars still study them separately in their research for simplicity. The definition of state variables through this form of non-material dependent study is very effective for studying heat conduction, material migration, wave propagation, and chemical reactions in single-phase media (solid, liquid, gas, etc.) or equivalent continuous media (saturated soil), while the correlation between

state variables and material variables is not negligible for multi-phase systems such as unsaturated soil. For instance, a reduction in the porous water content of an unsaturated earth implies a reduction in earth's hydraulic head, and the permeability coefficient of soil often depends on the amount of soil pore water content, so the state variable head must have a certain relationship with the material variable permeability coefficient. Therefore, according to the continuous medium theory, it is very necessary to use the material variable and state variable and their dependence to describe the state of multiphase system, so the selection of state variable and material variable is a more important basic work in saturated-unsaturated seepage theory.

Soil in its actual state often exists as a three-phase coexistence, i.e. a porous medium consisting of three phases: liquid water, air and a soil skeleton whose main component is mineral organic matter. In order to study the content of liquid water in the soil, it is often expressed by its proportional relationship to the total soil volume, with the following common expressions:

The ratio of the volume occupied by water in the earth $\Delta V_w$ and the overall quantity of the soil $\Delta V_o$. The formula is expressed as:

$$\theta_v = \Delta V_w / \Delta V_0 \tag{19}$$

The ratio of the quantity of water $\Delta V_w$ and pore quantity $\Delta V_v$ in the volume element of the earth body, indicating the size of the amount of water filled in the body pore. The formula is expressed as:

$$S_r = \Delta V_w / \Delta V_v \tag{20}$$

Relative Saturation $S_e$:

$$S_e = \frac{\theta - \theta_r}{\theta_s - \theta_r} \tag{21}$$

where $\theta$ is the volume moisture content at any time, and $\theta_r$ is the residual volume moisture content; $\theta_s$ is the saturated volume moisture content.

For typical saturated earth mechanics, the nice stress is regularly used as a necessary kingdom variable to describe the stress kingdom of the earth. Taishaki (1943) described the superb stress as the distinction between the complete stress and the pore water pressure, and its bodily which means is the stress on the soil skeleton. For unsaturated earth, the bodily which means of tremendous stress is the equal as that of saturated soils, however by using definition, there are variations between them. According to the tremendous stress principle, all pore pressures in saturated soils are phase of the whole

stress. However, the pore strain in unsaturated soils is typically negative, i.e., it is a tensile stress, and its contribution to the whole stress relies upon on the saturation of the soil and the measurement distribution of the pores. The pore strain in unsaturated soils is now not always a thing of the complete stress, which makes the evaluation of the stress kingdom in unsaturated earth some distance extra elaborate than in saturated earth.

For unsaturated soils, Bishop (1959) extended the classical effective stress equation for Taishaki bases by proposing the following effective stress equation for unsaturated soils:

$$\sigma' = (\sigma - u_a) + \chi(u_a - u_w) \tag{22}$$

The magnitude of the value of the material variable $\chi$ is closely related to the saturation, and there is a certain functional relationship between them however it is difficult to accurately measure this functional relationship experimentally. In this paper, the effective stress parameter is directly defined as the relative saturation for the convenience of the study:

$$\chi = S_e = \frac{\theta - \theta_r}{\theta_s - \theta_r} \tag{23}$$

### 3.4 Soil Water Suction

Soil water absorption refers to the negative pressure of soil water. Soil water usually forms a concave curved moon surface on its surface due to the adsorption and capillary action of the soil matrix, implying that its pressure is lower than the atmospheric pressure. If the atmospheric pressure is used as a reference, the pressure of soil water is negative [24]. For ease of use, negative pressure is defined as suction to eliminate the negative sign, so soil water suction is quantitatively equal to natural soil water negative pressure and is often referred to as soil absorption. The graph depicts the water absorption of the soil matrix.

Soil water suction is essentially described by pore water potential energy, i.e., soil water suction is generated as a result of the reduction of pore water potential energy in the soil body. If the effects of temperature, gravity, etc. are ignored, the factors that cause the reduction of pore water potential energy are mainly capillary action (water-gas interface), short-range adsorption (solid-liquid interface), and osmosis. For the capillary and short-range adsorption, due to their obvious effects and clear physical causes, the suction force from these two is often defined as matrix suction. As for the infiltration produced by solute dissolution in the pore water, the infiltration suction generated

by this part is often ignored because of its complex causes, difficulty in measurement, and small specific gravity. The matrix suction in unsaturated soils is often written in the following form:

$$S = u_{\mathrm{a}} - u_{\mathrm{w}} \tag{24}$$

From the above equation, for unsaturated soil, if $u_a = 0$, that is, the pore pressure is set to atmospheric pressure and as a reference zero point, according to the above equation substituted into the negative pore water pressure $u_w < 0$, will get positive matrix suction. It can be seen that matrix suction is closely related to soil moisture content, the greater the saturation, the smaller the matrix suction will be, and at the saturation state, the matrix suction is reduced to 0.

According to the traditional geomechanics, i.e., the concept of water head is used to describe the potential energy and pressure potential energy of water body in earth, the suction in unsaturated earth can also be expressed by using the capillary rise height, i.e., $S = h_w\gamma_w$. In this paper, we will use the negative pore pressure head and water content to describe the relationship between matrix suction and soil water content, i.e., the soil-water characteristic curve to be described below.

### 3.5 Soil Moisture Characteristic Curve

Rainwater infiltration into the slope surface reaches the diving surface through a saturated-unsaturated percolation process. The infiltration of rainwater into the slope surface will, by nature, lead to a reduction in the matrix suction in the non-saturated areas of the slope surface and, according to the Mohr-Coulomb shear strength criterion derived for non-saturated earth, a reduction in the shear strength of the soils that make up the slope surface, which in turn leads to a reduction in slope stability. The shear strength generated by matrix suction is included in the cohesion of unsaturated soils [25]. In the dry season, the stability coefficient increases due to negative pore water pressure (or matrix suction). In the continuation of the rainy season, the infiltration of rainwater into the slope leads to a decrease in matrix suction and therefore a decrease in cohesion, and the stability coefficient of the slope may decrease significantly. Among them, the water infiltration process is described by Richard's equation, which can be written as

$$(C + SeS)\frac{\partial p}{\partial t} + \nabla \cdot \left[-\frac{k_s k_r}{\mu}\nabla(p + \rho g D)\right] = F \tag{25}$$

The relationship between matrix potential and water content of soil water cannot be analyzed theoretically yet based on the basic properties of the soil, therefore, some empirical equations or simple models are commonly used to represent it. The representative Van-Genuchten model can be expressed as

$$K(h) = K_s \frac{\{1-(-\alpha h)^{n-1}[1+(-\alpha h)^n]^{-m}\}^2}{[1+(-\alpha h)^n]^{m/2}} \tag{26}$$

Where, *Ks* is the saturated permeability system; $\theta_r$ is the remnant water containing capacity. If the water containing capacity corresponding to the matrix potential ($h = -15000$ cm) at the stable depletion point is taken as $\theta_r$, it can meet the practical needs; $\theta_s$ is the saturated water containing capacity; $h$ is the earth suction; $h_c$ is a matrix potential constant; $h_b$ is the soil intake suction; $\lambda$, $m$, $n$ are empirical constants and $a$ is the fitting parameter, which is generally considered as the inverse of the soil intake value; where $m = 1 - 1/n$.

The percolation rate of water satisfies Darcy's law:

$$v = -\frac{k_s k_r}{\mu} \nabla(p + \rho g D) \tag{27}$$

Combined with the effective stress principle and the continuity equation of solid particle motion, we can obtain:

$$-\frac{k}{\mu S_e} \cdot \nabla(k_r \cdot \nabla p) + L\frac{\partial p}{\partial t} + \left(1 - \frac{1}{S_e}\right)\frac{\partial \theta}{\partial t} = 0 \tag{28}$$

$$L = \left(\frac{\theta}{S_e} - 1\right) \cdot \frac{2}{G(1+v)} + \theta\beta_w + \left(1 - \frac{\theta}{S_e}\right)\beta_s \tag{29}$$

Equation (28) is the flow-solid coupling model under rainwater infiltration conditions, where $\theta$ is the volumetric water content; $\beta_s$ is the solid skeleton compression coefficient.

## 4 Experiment and Simulation

### 4.1 Design for Working Conditions

Table 2 shows the rainfall class classification standards stipulated by relevant codes in China. In this paper, the changes of transient seepage field of slope under various rainfall levels will be considered comprehensively, and the

**Table 2** Rainfall rating table

| Serial Number | Rainfall Levels | Phenomenon Description | Rainfall Range | |
|---|---|---|---|---|
| | | | Total in One Day | Total in Half a Day |
| 1 | Light rain | The ground is wet, but not muddy | 1–8 | 0.4–4 |
| 2 | Mid Rain | There is a pattering sound on the roof and water accumulates in the alcove | 8–26 | 4.1–16 |
| 3 | Heavy Rain | Rainfall like pouring, water accumulates on the flat | 26–52 | 16.1–30 |
| 4 | Rainstorm | Rainfall can cause flash floods | 52–100 | 30.1–65 |
| 5 | Heavy rainstorm | Rainfall prone to flooding | 100–200 | 65.1–130 |
| 6 | Extraordinary rainstorm | Longer period of time | >200 | >140 |

rainfall intensity taken mainly covers four levels: medium rain, heavy rain, heavy rain and big rainstorm.

The Longlian Expressway project studied in this paper has a mid-subtropical monsoon climate. The main characteristics of the climate are: long summer and winter, short spring and autumn, mild climate, four distinct seasons, sufficient light, abundant heat, abundant rainfall, and obvious precipitation seasons. The average temperature throughout the year hovers between 18.0°C and 20.7°C. The average temperature in January is the smallest, generally between 9.2°C and 10.8°C; the average temperature in July is the largest, usually between 26.3°C and 28.0°C.

## 4.2 Analysis of Rainfall on Slope Stability of Road Graben

In order to obtain the pressure head variation of the main part of the slope under different working conditions, the pressure head distribution data of the model under four rainfall intensities were extracted according to four cross sections, and the variation of pressure head along the slope depth of the four control sections were plotted as shown in Figure 5.

As shown in Figure 5, different rainfall intensities have different effects on the seepage field of the slope body. The head pressure of A-A and B-B sections eventually drops to about 10, the head pressure of C-C sections eventually drops to around 16, and the head pressure of D-D sections eventually drops to 20. (1) For the soil at the foot of the slope, due to the low permeability coefficient and the limited depth of rainfall infiltration, the change of seepage field is not obvious. (2) For the soil near the top of the

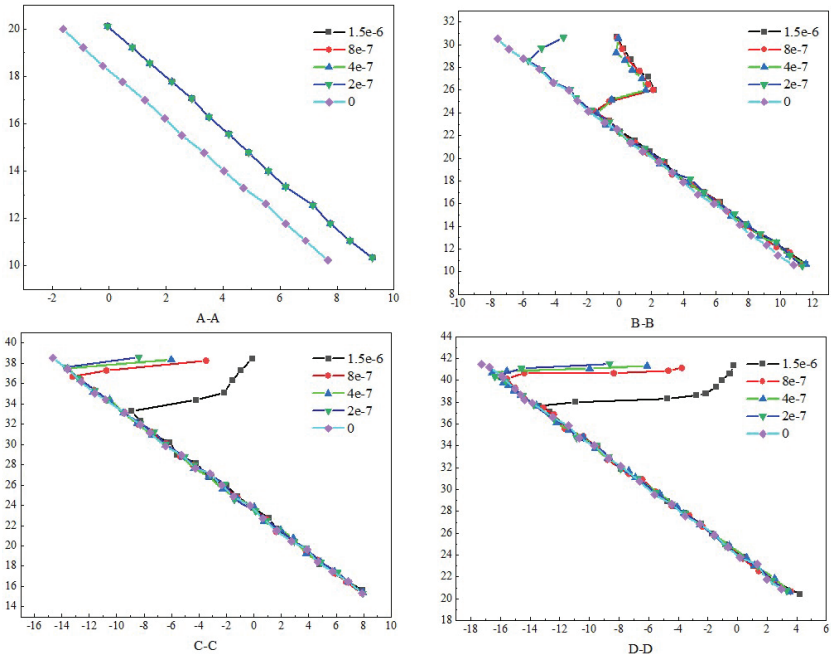


**Figure 5** Pressure head distribution of the four control sections.

slope, due to the large permeability coefficient, different rainfall intensities directly affect the distribution of the seepage field of the slope body, and generally large rainfall intensities cause more matrix suction loss and deeper infiltration depth. (3) The pressure head at the partition interface in the slope body where the permeability coefficient changes will occur inflection point, and the pressure head distribution at the partition interface shows a different form of distribution from the pressure head of homogeneous slope.

The conditions TM1∼TM6 are considered when the rainfall intensity is set to 4 $e^{-7}$ m/h and the rainfall duration is 6 h, 12 h, 24 h, 36 h, 48 h, and 72 h respectively for the seepage field of the slope. Since the rainfall duration is long, if the drainage boundary is not set, the seepage field in the slope body will be different from the actual seepage field, so a drainage boundary with pore pressure of 0 is set in the range of about 2 m at the foot of the slope.

As shown in Figure 6, the influence of rainfall holding time on the seepage field is as follows: (1) The longer the rainfall holding time is, the deeper the infiltration depth will be, while the rainfall will continuously replenish the groundwater. (2) The influence of different lengths of rainfall holding

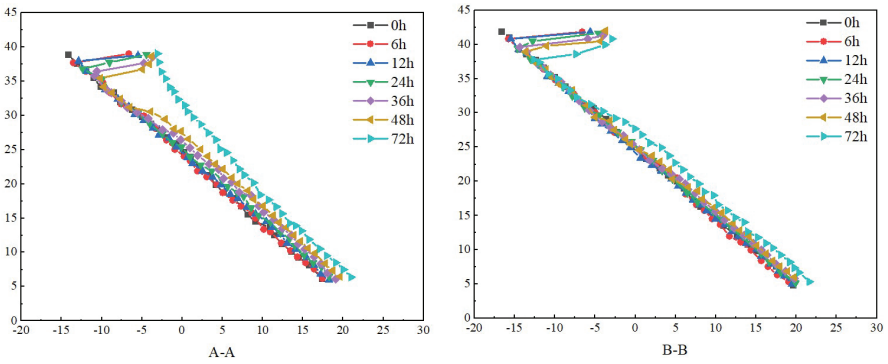


**Figure 6** Pressure head distribution of the control section at different moments.

time on different parts of the slope body is different, basically the influence on the upper part of the slope body is richer than the influence on the lower part of the slope body.

In order to find out about the affect of rainfall infiltration on the steadiness of the slope containing weakly interbedded carbonaceous shale, a slope mannequin with a 30° inclination of weakly interbedded shale used to be used as an example, and the alternate of slope steadiness coefficient with rainfall time used to be calculated numerically beneath distinctive rainfall intensities. The steadiness coefficient of the slope is evaluated by way of the calculated steadiness coefficient of the slope, and the calculated steadiness coefficient of the slope bought by way of simulation is proven in Figure 7. The trade regulation of balance coefficient of the slope containing weakly interbedded carbonaceous gentle rock in the direction of 96 h rainfall is as follows: 1. When the rainfall depth is certain, the infiltration of rainwater in the soil will increase continually with the rainfall time, the saturation of the slope soil step by step will increase from the floor layer to the interior layer, the pore water strain increases, the shear energy decreases, and the steadiness coefficient of the slope steadily decreases. 2. Under distinct rainfall intensities, the exchange fashion of slope steadiness with the rainfall time is greater or much less the same, and the balance coefficient of the slope decreases constantly with the rainfall time. The higher the rainfall intensity, the higher the slope of the balance coefficient curve, i.e., the quicker the balance coefficient decreases. At the rainfall depth of 10.0 mm·h$^{-1}$, the slope balance coefficient curve slope indicates the alternate regulation of steep first and then slow, the balance coefficient of slope declines quick at the early stage of rainfall, and after 60 h of rainfall, the steadiness coefficient of slope

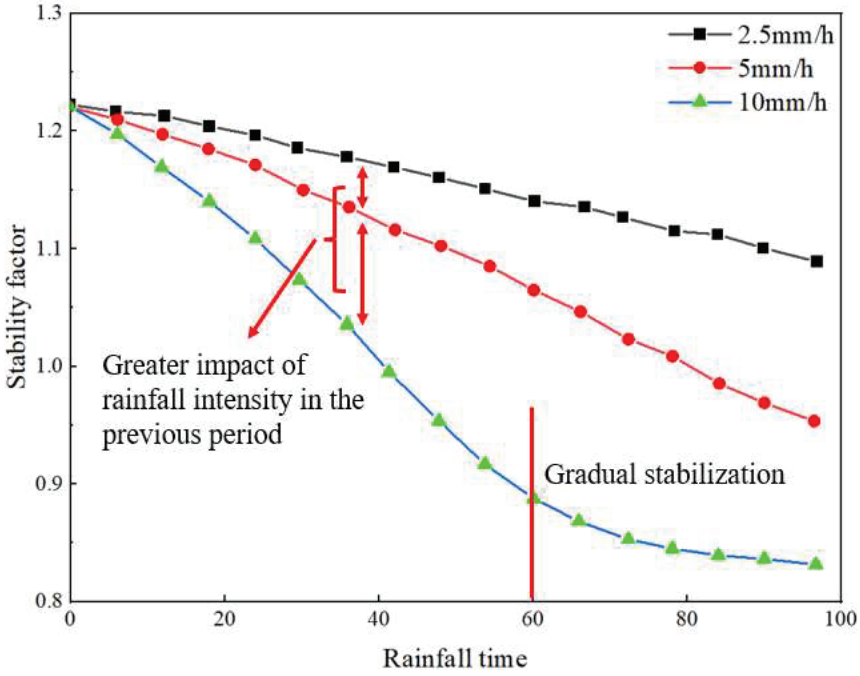


**Figure 7** Curve of slope stability coefficient with time.

declines step by step and slowly. Finally, it tends to be stable, which shows that the rainfall depth has a larger have an effect on the steadiness coefficient of slope in the early rainfall process, and the foremost thing affecting the limit of balance coefficient of slope in the late rainfall is no longer the rainfall intensity. And when the rainfall depth is 2.5 mm·h$^{-1}$ and 5.0 mm·h$^{-1}$, the price of decline of slope balance coefficient in late rainfall is essentially the equal as that in early rainfall.

Under the condition of rainfall intensity of 10.0 mm·h$^{-1}$, the stability of the slopes containing soft and weak interlayer with inclination angles of 25°, 30° and 35° is simulated and the relationship between slope stability coefficient and rainfall time is obtained, which is detailed in Figure 8.

It can be seen from Figure 8 that the slope stability of different weak interlayer dip angles has roughly the same variation trend with the rainfall time, and the slope stability decreases with the increase of rainfall time. When the dip Angle of the weak interlayer is equal to 25°, the initial stability coefficient of the slope is the maximum, and the stability coefficient decreases rapidly with the rainfall time. When the rainfall reaches 60 h, the

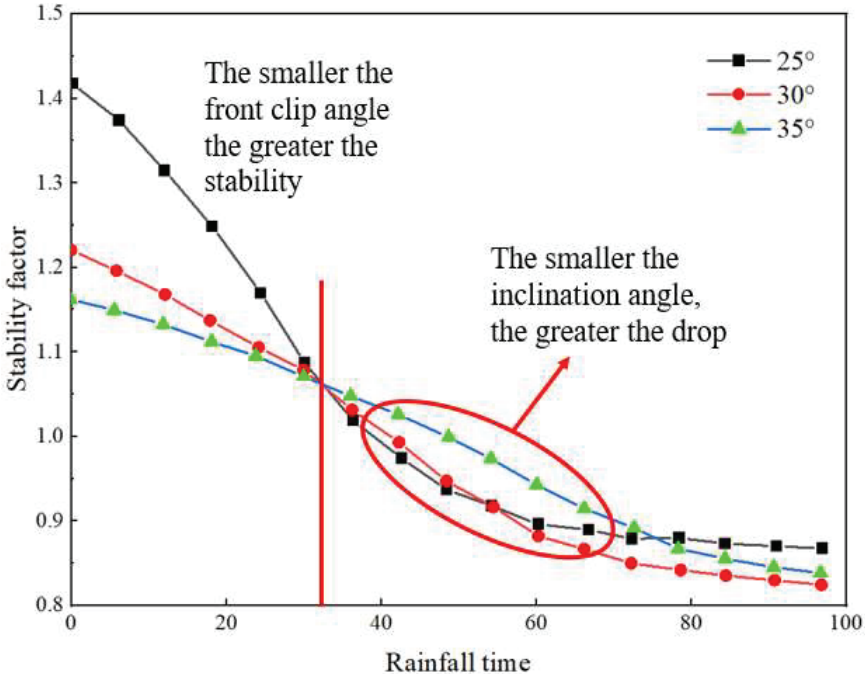


**Figure 8** Stability curves with time for different inclination angles.

stability coefficient becomes stable. When the dip Angle is 30°, the stability coefficient decreases rapidly with the rainfall time to 72 h and then becomes gentle. When the dip Angle is 35°, the slope stability decreases linearly with time at a certain slope. Although the stability coefficient of slope decreases gradually with rainfall time. But from the slope of the curve, the slope of the 25° dip Angle is the largest, which means that its stability coefficient decreases the fastest and it is affected by rainfall the most. It can be seen that, under the same rainfall intensity, the smaller the dip Angle of weak sandwich, the faster the slope stability decline, the greater the decline, that is, the smaller the dip Angle, the greater the impact of rainfall on slope stability. According to the analysis of rainfall infiltration process, the lower the slope dip Angle, the farther the surface of the interlayer is from the slope shoulder, the longer the weak interlayer, the more water, the greater the increment of soil body weight above the weak interlayer. At the same time, the shear strength of soil decreases due to the decrease of effective stress. Therefore, in the range of the dip Angle of the weak interlayer of 25°∼35°, the same rainfall time and rainfall intensity, the smaller the dip Angle of the weak interlayer, the greater

the impact on slope stability, the smaller the dip Angle, the greater the initial stability, the greater the stability reduction range, the slope is very likely to destabilization failure.

## 5 Conclusion

In this paper, the right graben slope from K316+439 to K316+859 of Longlian Expressway is selected, and the monitoring points are arranged to monitor the deep horizontal displacement with the help of tilt holes, and then the force and stability analysis of the graben slope under the rainfall condition is carried out based on the saturated-unsaturated seepage theory. The specific results are as follows:

1. The damage mode of the road graben slope and its damage stages are summarized, i.e. three damage stages of creeping deformation, sliding damage and tending to stability. Rainfall gradually penetrates from the dense solid surface, and usually the water content can be divided into four regions from the surface to the inside, saturated region, transition region, conduction region and wetting region.
2. The continuity assumption is proposed from microscopic and macroscopic aspects, and the two-dimensional transient seepage control equations are derived based on saturated-unsaturated seepage theory. The state variables of soil water and material variables as well as the soil matrix suction analysis were selected based on the continuous medium theory, and the flow-solid coupling mathematical model and soil moisture characteristic curve model under rainfall infiltration conditions were proposed.
3. The pressure head at the partition interface in the slope body where the infiltration coefficient changes will be inflected, and the pressure head distribution at the partition interface shows a different form of distribution from the pressure head of homogeneous slope. The influence of different lengths of rainfall holding time on different parts of the slope body is different, basically the influence on the upper part of the slope body is more abundant than that on the lower part of the slope body. At the rainfall intensity of 10.0 mm-h-1, the slope stability coefficient curve slope shows a steep and then slow change law, the stability coefficient of the slope decreases fast at the early stage of rainfall, after 60 h of rainfall, the stability coefficient of the slope decreases gradually and the force equilibrium of the road graben slope no longer changes.

## References

[1] Yao S Z, Li G D, Zhang F X, et al. Study of highway crack diagnosis based on cellular neural network[C]//Applied Mechanics and Materials. Trans Tech Publications Ltd, 2013, 427.

[2] Hearn G J. Some of the geological challenges and opportunities associated with the dynamics of the Cenozoic East African Rift System[J]. Quarterly Journal of Engineering Geology and Hydrogeology, 2022, 55(3).

[3] Yang X. Numerical analysis of seepage characteristics of high slopes of road graben with soft sandwich under rainfall infiltration conditions[J]. Chinese and foreign highways, 2020, 40(4): 38–42.

[4] Pan H. Application of Multi Body System Coupling Dynamic Model in Posture Stability Evaluation of Sports[J]. European Journal of Computational Mechanics, 2021: 81–98.

[5] Xu Haitao, Liang Chao. Stability analysis of cascading slopes under rainfall conditions[J]. Advances in Water Resources and Hydropower Technology, 2013, 33(5): 73–76.

[6] Paul K, Mukhopadhyay B. Transient Dynamic Response of a Semi-infinite Elastic Permeable Solid with Cylindrical Hole Subject to Laser Pulse Heating Under Different Theories of Generalized Thermoelasticity[J]. European Journal of Computational Mechanics, 2020: 517–548.

[7] Yu Jinhui. Trend analysis of safety coefficient changes of high road graben slopes under the effect of strong rainfall[J]. Mining and Metallurgical Engineering, 2014, 34(3): 23–25.

[8] Rezaiee-Pajand M, Naserian R, Afsharimoghadam H. Two Ways of Solving System of Nonlinear Structural Equations[J]. European Journal of Computational Mechanics, 2019: 433–466.

[9] Rosa P M C. Procedural modelling techniques to configure driving serious game scenes[J]. 2015.

[10] Li Shiwen. Research on stability analysis and support measures of highway rift valley high side slopes[J]. Highway Engineering, 2018, 43(5): 163–168.

[11] Jia Z, Wu H, Peng J, et al. The deep origin of ground fissures in the Kenya Rift Valley[J]. Scientific Reports, 2023, 13(1): 3672.

[12] Vereschaka A, Tabakov V, Grigoriev S, et al. Investigation of the influence of the thickness of nanolayers in wear-resistant layers of Ti-TiN-(Ti, Cr, Al) N coating on destruction in the cutting and wear of carbide cutting tools[J]. Surface and Coatings Technology, 2020, 385: 125402.

[13] Oinam M, Rajkumar H S, Soibam I, et al. Sedimentary petrography and ichnology of the Barail Group along the Old Cachar road, Manipur, India[J]. Arabian Journal of Geosciences, 2022, 15(8): 706.
[14] Rubingh K E, Gibson H L, Lafrance B. Evidence for voluminous bimodal pyroclastic volcanism during rifting of a Paleoproterozoic arc at Snow Lake, Manitoba[J]. Canadian Journal of Earth Sciences, 2017, 54(6): 654–676.
[15] Hu JC, Xie YL, Wang WS. Stability test of stepped loess slopes under rainfall conditions[J]. Journal of Guangxi University: Natural Science Edition, 2010 (1): 83-89.
[16] Kumaar S, Mannar S, Navaneethkrishnan B, et al. High Speed Autonomous Navigation of Unmanned Aerial Vehicles using novel Road Identification, Following & Tracking (RIFT) Algorithm[C]//2019 IEEE International Conference on Distributed Computing, VLSI, Electrical Circuits and Robotics (DISCOVER). IEEE, 2019: 1–6.
[17] Aksenov V V, Efremenkov A B, Sadovets V Y, et al. Impact of the number of blades of the geokhod cutting body on the energy intensity of the rock destruction[C]//IOP Conference Series: Materials Science and Engineering. IOP Publishing, 2019, 656(1): 012002.
[18] Shishlyannikov D, Zvonarev I. Investigation of the destruction process of potash ore with a single cutter using promising cross cutting pattern[J]. Applied Sciences, 2021, 11(1): 464.
[19] Zhang JP. Stability analysis of road graben slopes considering the effect of heavy rainfall[J]. Guangdong Transportation Planning and Design, 2017 (3): 23–26.
[20] Dindi E. An assessment of the performance of the geophysical methods as a tool for the detection of zones of potential subsidence in the area southwest of Nakuru town, Kenya[J]. Environmental Earth Sciences, 2015, 73: 3643–3653.
[21] Lan J. Seismic Design of Dillon Road Grade Separation Bridge[M]// Sustainable Transportation Systems: Plan, Design, Build, Manage, and Maintain. 2012: 515–522.
[22] Wu Bo-Hong, Mo Jiang. Stability analysis of rainfall infiltration in swelling soil road graben slopes[J]. Building Structures, 2016 (S1): 851–855.
[23] Wu T, Jia J, Jiang N, et al. Model test of deformation evolution and multi factor prediction of anchorage slope stability under rainfall condition[J]. Journal of Earth Science, 2020, 31: 1109–1120.

[24] Yuan H P, Chen S M, Zhu D Y, et al. Slope stability analysis of loose rock pile graben under heavy rainfall excitation[J]. Journal of Hefei University of Technology: Natural Science Edition, 2015, 38(6): 799–803.
[25] Fredlund D G. Unsaturated soil mechanics in engineering practice[J]. Journal of geotechnical and geoenvironmental engineering, 2006, 132(3): 286–321.

## Biographies

**Li Peijun** received the master's degree in engineering from Chang'an University in 2019. He is currently working as an engineer at the Department of geotechnical engineering of Guangdong Transportation Technology Testing Co., Ltd. His research areas and directions include slope and tunnel safety monitoring system, disaster prevention and mitigation, application of new technology in geotechnical engineering.

**Lu Hao** received the doctor's degree in engineering from Chang'an University in 2018. He is currently working as an engineer at the Department of

geotechnical engineering of Guangdong Transportation Technology Testing Co., Ltd. His research areas and directions include slope safety monitoring, consulting evaluation, and disaster prevention and research.

**Li Qing** received the master's degree in engineering from Chang'an University in 2006. He is currently working as an senior engineer at the Department of geotechnical engineering of Guangdong Transportation Technology Testing Co., Ltd. His research areas and directions include slope and tunnel safety monitoring, consulting evaluation and maintenance of reinforcement design.